Version of Record: https://www.sciencedirect.com/science/article/pii/S0166516222002427
Manuscript_9fd266ca33a3decca52268db72115239

Uniformity and volume-representativity of consecutive submillimetre wafers of shale for SANS and USANS investigations

Yeping Ji[a], Andrzej P. Radlinski[a], Tomasz Blach[a], Phung Vu[a], Mengdi Sun[d], Liliana de Campo[b], Elliot P. Gilbert[b], Hamid Roshan[a] and *Klaus Regenauer-Lieb[c,a]

[a]School of Minerals and Energy Resource Engineering, Kensington, University of New South Wales, Sydney, NSW 2052, Australia
[b]Australian Centre for Neutron Scattering, Australian Nuclear Science and Technology Organisation, New Illawarra Road, Lucas Heights, NSW 2232, Australia
[c]WA School of Mines: Minerals, Energy and Chemical Engineering, Curtin University, Perth, WA 6102, Australia
[d]Key Laboratory of Continental Shale Hydrocarbon Accumulation and Efficient Development, Ministry of Education, Northeast Petroleum University, Daqing 163318, China

Abstract

(Ultra) Small Angle Neutron Scattering (SANS/USANS) is a non-destructive technique suitable for characterization of porous structures from nano- to micro-pore size (1 nm to 20 μm), which has been widely used to characterize accessible and inaccessible porosity in tight unconventional hydrocarbon reservoirs (e.g., shales). In this study, SANS and USANS are used to examine the degree of nano- to micropore uniformity of the rock body on sub-millimetre to centimetre scale. This study presents a test of the hypothesis of volume representativity of pore structure information measured by SANS and USANS for shale wafers (0.22-1 mm) cut from six North American unconventional shale cores of different maturities (New Albany Shale and Marcellus Shale). Experimental reproducibility of USANS is further investigated for two wafers measured using various acquisition times. All samples show that fluctuations of the relative intensity generally decrease from the USANS Q-range (pore size from around 200 nm to 20 μm) to most of the SANS Q-range (pore size from around 5 nm to 700 nm), and peaks in the SANS large-Q region (for pores smaller than about 5 nm). There is a positive correlation between the spatial fluctuation of the relative SANS intensity and the scattering power of shales. In addition, the scattering intensity and its fluctuations is larger for the less mature shale cores. Shale is known to be highly heterogenous and the hypothesis of uniformity does not apply at sub-millimetre scale

© 2022 published by Elsevier. This manuscript is made available under the Elsevier user license
https://www.elsevier.com/open-access/userlicense/1.0/

even for samples that appear homogeneous at visual inspection. This study presents an approach to minimise the variation through sample selection, data interpretation methodology and instrumental reproducibility tests. The best values of the microstructural spatial uniformity for the apparently homogeneous sections of a core (i.e., the SANS and USANS intensity variation) is less than ±10%.

Keywords: SANS and USANS, shale, consecutive wafers, uniformity, volume-representativity

1. Introduction

Pore structure information in unconventional reservoir rocks is important for hydrocarbon recovery in petroleum industry (Sun et al. 2020). Due to its low carbon footprint and abundant reserves, shale gas is considered a transitional energy source for the period of continued reduction of greenhouse gas emissions (Warpinski et al. 2009, Considine et al. 2010, Sieminski 2021). However, production of hydrocarbons from unconventional tight formations is technically difficult and carries a significant economic and potential environmental cost (Lee et al. 2011, Cao et al. 2017, Silva et al. 2017, Radlinski et al. 2021, Sun et al. 2021). Most of the unconventional reservoirs have ultra-low permeabilities and porosities (Warpinski et al. 2009, Sander et al. 2017, Radlinski et al. 2021, Sun et al. 2022) and multiscale pore structures (from sub-nanometres to micrometres) (Clarkson et al. 2013, Melnichenko 2016, Sun et al. 2020, Blach et al. 2021); majority of hydrocarbons volume is trapped in the nano- and micropores (Sun et al. 2016, Blach et al. 2020). The entrapment of gas in the tight pore space is argued to be the reason for the low gas recovery (≤ 30%) obtained using the current fracturing methods (You et al. 2017, Sun et al. 2021). The migration, production and recovery rates are impacted by pore characteristics in the reservoir rocks (Chiang et al. 2018, Sun et al. 2020).

Multiple techniques are required to systematically study the multiscale pore structure of unconventional reservoir rocks (Clarkson et al. 2013). Various experimental techniques have been used to characterize pore structure, including nuclear magnetic resonance (NMR) (Bowers et al. 2019), imaging methods (FE/FIB-SEM, TEM, STM, AFM) (Gu et al. 2015, Chen et al. 2020, Sun et al. 2020, Ge et al. 2022, Wang et al. 2022), high-pressure mercury intrusion and low-pressure gas (CO_2 or N_2) adsorption (Melnichenko et al. 2009, Clarkson et al. 2012, Clarkson et al. 2013, Sun et al. 2017, Liu et al. 2019). Each of these methods has limitations, such as finite range of pore sizes and a specific pore geometry assumed during interpretation of experimental data which makes it difficult to combine (and directly compare) the results. In addition, there are issues specific to invasive measurements, such as possible nano-structural damage caused by high pressures of mercury and differences in physical sizes of the Hg, N_2 and CO_2 molecular probes. Importantly, these techniques are not capable of examining the inaccessible (closed) pore space (Radliński et al. 2000, Clarkson et al. 2013, Bahadur et al. 2016, Melnichenko 2016, Sun et al. 2016, Sun et al. 2020, Radlinski et al. 2021).

In contrast, (Ultra) Small-angle Neutron Scattering (SANS/USANS) is a non-destructive technique overcoming many of the above problems for pore characterization: (1) USANS combined with SANS can investigate the pore size scale from ~1 nm to around 20 μm; (2) various types of samples can be used, such as free-standing solid sample slices (sensitive to directional rock matrix anisotropy) or coarse grains (for which the azimuthally averaged SANS profile reflects the spatially averaged rock matrix microstructure); (3) contrast matching techniques combined with SANS and USANS techniques effectively distinguish open and closed pores, accessible or inaccessible to the matching fluids (Radlinski 2006, Jackson et al. 2008, Anovitz et al. 2009, Sakurovs et al. 2012, Anovitz and Cole 2015, Bahadur et al. 2016, Melnichenko 2016, Sun et al. 2016, Sun et al. 2020, Radlinski et al. 2021). For these reasons, well-prepared volume-representative samples are necessary.

Based on recent research on the multiple scattering (MS) effects in rocks and the consequent distortion of the absolute scale experimental SANS and USANS results (Ji et al. 2022), the optimal sample thickness for MS-minimised data is in the sub-millimetre range (around 0.5 mm, depending on the scattering power of sample materials). However, there is no systematic study on volume-representativity and uniformity of such prepared thin wafers.

Due to the high cost and limited availability of SANS and USANS instruments, it is a common practice to limit analysis to a single wafer which has been cut from a core sample that appears homogeneous under visual inspection. The general assumption then is to take this single wafer as a representative sample for the entire core. The Australian Nuclear Science and Technology Organisation (ANSTO) allocated beam time to our group to perform the first verification of this fundamental assumption, sufficient to measure 43 wafers of six sets of shales. These results were needed to test compatibility of SANS and USANS measurements which by necessity were performed on different samples due to destructive experimental conditions (e.g., high-pressure, high-temperature and solvent application, etc).

In this study, systematic SANS and USANS measurements were performed for consecutive sample wafers sliced from six shale cores with various organic matter content and different thermal maturity. The primary aim is to examine the nano- and microstructure uniformity and volume-representativity of thin wafers ($t \approx 0.2 - 1.0$ mm) of the rock under investigation at SANS and USANS regions. This study thereby intends to provide a solid basis for future quantification of variability of the population density of scatterers, used for subsequent upscaling studies from core scale to reservoir scale. It is particularly important as an input data set for a variety of explicit numerical upscaling methods including the

calculation of upper and lower bounds of physical properties at the reservoir scale (Liu and Regenauer-Lieb 2021).

2. Background of small angle neutron scattering

SANS and USANS (Agamalian et al. 1997) are established techniques for microstructural research on geological materials (Schmidt 1982, Bale and Schmidt 1984, Wong et al. 1986, Lucido et al. 1988, Winans and Thiyagarajan 1988, Schmidt et al. 1989, Allen 1991, Radliński et al. 1999, Radliński et al. 2000, Melnichenko et al. 2009, Clarkson et al. 2013, Bahadur et al. 2016, Sun et al. 2018, Blach et al. 2021). Radlinski et al. (1996) originally proposed to use SANS to detect hydrocarbon generation in tight mudstones. Theoretical foundations for interpretation of scattering from shale have been developed by Radliński et al. (2000), Radlinski (2006), Melnichenko (2016), Jackson et al. (2008), Sun et al. (2020) and Radlinski et al. (2021).

The basic principle of scattering is expressed as the relationship between the scattering intensity I(Q) and the neutron scattering vector Q ($Q = 4\pi\sin\theta/\lambda$), where 2θ is the scattering angle between the incident and scattered beams and λ is the neutron wavelength (Melnichenko et al. 2009, Anovitz and Cole 2015, Sun et al. 2020). For many sedimentary rocks a two-phase approximation can be used for data interpretation; this simplification is a consequence of the similar scattering length density (SLD) for various solid inorganic and organic rock components and significant difference of SLD between the solid rock matrix and the pore content (Radliński et al. 2000, Melnichenko 2016, Sun et al. 2018). The differential scattering cross-section $(d\sigma/d\Omega)(Q)$, equivalent to the intensity I(Q)) is expressed as:

$$\frac{d\sigma}{d\Omega}(Q) \equiv I(Q) = \overline{\Delta\rho^2} V_0 S(Q) \quad (1)$$

where $\Delta\rho$ is the function of SLD difference between the rock matrix (ρ_m) and the pore space (ρ_s), V_0 is the average pore volume, S(Q) is the structure factor and

$$\overline{\Delta\rho^2} = (\rho_m - \rho_s)^2 \Phi(1 - \Phi) \quad (2)$$

where Φ is total porosity. The SLD for any particular rock matrix (ρ_m) is given by a closed formula (Radlinski et al. 1996); it can be calculated using the NIST SLD calculator, based on the bulk density and empirical chemical formulas and volume fraction of each compound in the rock matrix (https://www.ncnr.nist.gov/resources/activation/); details for rocks used in this study have been described elsewhere (Ji et al. 2022).

In this study, we interpret SANS and USANS results using the Porod Invariant (for total porosity) and the Polydisperse Spheres structural model (PDSP) which assumes that the shape of pores is spherical (spatially isotropic). Detailed calculations were performed using

142 the PRINSAS software (Radliński et al. 2000, Hinde 2004, Bahadur et al. 2015), based on the
143 following formula (Espinat 1990, Zhang et al. 2020, Blach et al. 2021):

144 $$I(Q) = (\rho_m - \rho_s)^2 N_0 \int_0^\infty f(r)\,[v(r)]^2\,F_0(Q,r)dr \quad (3)$$

145 where N_0 is the concentration of pores, f(r) is the probability density distribution for pore
146 sizes, $v(r) = \frac{4}{3}\pi r^3$ is the pore volume and F_0(Q,r) is the form factor of spheres with a radius
147 r normalised to unity at Q=0.

148 Given the power law I(Q) (fractal-like) scattering of rocks studied here, we use a
149 model-independent Bragg-law-like approximate relationship between the pore radii r* that
150 dominate the scattering intensity and the corresponding scattering vector Q: $r^* \approx 2.5/Q$
151 (Radliński et al. 2000, Melnichenko et al. 2012, Sun et al. 2020). Subsequently, the total
152 porosity (Φ), the probability density distribution for pore sizes, f(r), specific surface area for
153 various molecular probe sizes, SSA(R) and the incremental pore volume ((dV/dr)(r)) have
154 been estimated.

3. Experimental Methods

3.1 Samples

Five New Albany Shale (SDH-308, McAtee-2798, Gibson-3997, Hardin-IL2, and Hardin-IL3) rocks and one Marcellus Shale (Marcellus-7084) rock have been measured (Table 1), with organic matter maturity ranging from immature to post-mature (vitrinite reflectance (R_o), a measure of thermal maturity of the organic matter, ranging from 0.5% to 1.41% for the New Albany Shale samples and R_o = 2.5% for the Marcellus Shale sample). Samples of Hardin-IL2 and Hardin-IL-3 were obtained from outcrops and their maximal sample depths have been estimated from the corresponding Ro values; full information has been published elsewhere (Blach et al. 2021, Radlinski et al. 2021). In total, 43 wafers have been prepared; all were measured at ambient conditions using SANS and 17 using USANS (Table 2 and Supplementary Material B). The details for all samples are provided in Supplementary Material A1, A2 and A3.

Table 1. Shale sample information. The sample depth for Hardin-IL2 and Hardin-IL3 is only approximate.

Abbreviated sample name	**R_o (%)**	**Total Organic Carbon (TOC) (weight%)**	**Organic matter maturity**	**Sample Depth (m)**	**Sample location**
SDH-308	0.5	14.4	immature	75.3	Harrison County, Indiana
McAtee-2798	0.7	6.6	mid-mature	852.8	Pike County, Indiana
Gibson-3997	0.84	5.9	mid-mature	1218.3	Gibson County, Indiana
Hardin-IL2	1.04	8.4	late mature	1402.1	Hardin County, Illinois
Hardin-IL3	1.4	3.6	post-mature	1645.9	Hardin County, Illinois
Marcellus-7084	2.5	3.4	post-mature	2159.2	Pennsylvania

171 Table 2. Number and thickness range of shale wafers used in this study. Full details are
172 provided in Supplementary Material B.

Sample type	SANS		USANS	
	Number of wafers	Thickness range (mm)	Number of wafers	Thickness range (mm)
SDH-308	9	0.68 - 0.92	not done	not done
McAtee-2798	5	0.79 - 0.83	3	0.79
Gibson-3997	8	0.81 - 0.94	3	0.84 - 0.90
Hardin-IL2	8	0.57 - 0.83	3	0.79 - 0.80
Hardin-IL3	8	0.76 - 0.87	3	0.79 - 0.82
Marcellus-7084	5	0.22 - 1.00	5	0.22 - 1.00

173

3.2 Instruments and Data Processing

SANS and USANS measurements were conducted at the Australian Centre for Neutron Scattering of the Australian Nuclear Science and Technology Organization (ANSTO), Lucas Heights, New South Wales, Australia. Three instruments were used: a double-crystal USANS instrument (Kookaburra), a 40m monochromatic SANS instrument (Quokka), and a time-of-flight (TOF) SANS instrument (Bilby). For USANS measurements, two neutron wavelengths (λ = 2.37 Å and 4.74 Å) were used, which cover the Q range from 1.5×10^{-5} to 2×10^{-3} $Å^{-1}$ (Rehm et al. 2013). For the pinhole SANS instrument Quokka (Gilbert et al. 2006, Wood et al. 2018), in total four configurations were used to cover the Q-range from 6×10^{-4} to 0.5 $Å^{-1}$ with 10% wavelength resolution: (1) MgF_2 focussing lens (λ = 8.1 Å) at the sample to detector distance (SDD) equal to the source to sample distance (SSD): SDD = SSD = 20 m; (2) SDD = SSD = 20 m, λ = 5 Å; (3) SDD = SSD = 8 m, λ = 5 Å and (4) SDD = 1.3 m, SSD = 4 m, λ = 5 Å. For the TOF SANS instrument (Bilby), neutron wavelengths from 2 Å to 20 Å were used to cover the Q-range from ~1×10^{-3} $Å^{-1}$ to ~1.5 $Å^{-1}$; the scattering intensity has been simultaneously measured for the full wavelength range, with an option to perform data reduction using an arbitrarily selected wavelength range (Sokolova et al. 2019, Ji et al. 2022). Prior to the measurements proper, the background scattering intensity (from empty beam and empty cell) was measured and subtracted from experimental data (Kline 2006, Jackson et al. 2008, Melnichenko 2016, Ji et al. 2022, Sun et al. 2022). Intensity profiles were confirmed to be isotropic and were radially averaged and reduced to absolute units using laboratory-provided standard software packages: Python scripts were written for the analysis software Gumtree for USANS data reduction (Xiong et al. 2017) and Mantid for desmearing (Arnold et al. 2014). NCNR macros written in IGOR software and modified for the pinhole SANS (Quokka) data reduction (Kline 2006, Wood et al. 2018), and Python scripts written in Mantid for the TOF SANS (Bilby) data reduction (Arnold et al. 2014).

For SANS, the experimental statistical errors (error bar at 1-sigma) in the initial files are determined by averaging the 2D to 1D data and thus, with increasing Q, a greater number of pixels are utilised in the averaging; this, however, is not compensated by the rapidly decreasing scattering function. It is important to note that other factors (instrument configuration) also contribute to statistical uncertainty. For USANS, the experimental statistical errors are determined by counting statistics at each point which is typically targeted to be 3% (1000 neutron counts per Q-value). To calculate relative intensity variations, the 1D data for each dataset were averaged, and then each curve was normalised by this average at

each fixed Q, always using standard error propagation as implemented in Mantid (Arnold et al. 2014). The standard deviation (Altman and Bland 2005) is used to calculate the scattering intensity variation (sigma variation) and measurement statistical errors (sigma uncertainty). The dominant contributor to the overall variation is then quantitatively analysed as the variation dominated by the sample heterogeneity can be approximated by a difference between the squared sigma variation and the squared sigma uncertainty.

4. Results and Discussion

4.1 SANS and USANS results

In this section, SANS results for six sets of consecutive shale wafers and USANS results for five of the sets are presented. For each set of wafers, we examine the reproducibility of the scattering intensity and the consequent uniformity of the nano- and microstructure of the original rock core on a sub-millimetre to centimetre scale. In addition, the variability of USANS results (which is generally larger than the scatter of the corresponding SANS results) was investigated by repeated measurements of the same sample.

4.1.1 SANS results for SDH-308 wafers

The SDH-308 wafers sliced from the immature New Albany Shale core originating from Harrison Country, Indiana. The sample depth is 75.3 m, Total Organic Carbon (TOC) is 14.4 weight % and the thermal maturity of organic matter is low (R_o is 0.5%; Table 1). The thickness of wafers ranges from 0.68 mm to 0.92 mm (Table 2 and Table B1); the physical appearance of the opposing large faces for each wafer is illustrated in Figure 1 (SANS and USANS measurements characterise the bulk of each slice and were performed with a randomly selected face exposed to the incident beam of neutrons). The inconsistent order of sample names is due to the loss of some samples in previous destructive studies.

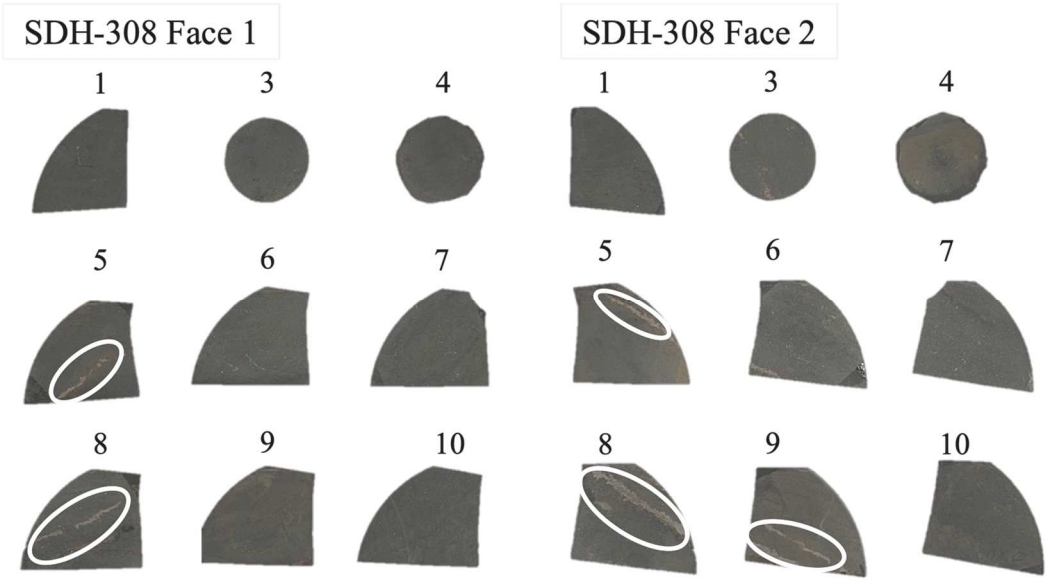

Figure 1. Sample physical appearance (two large faces) for SDH-308 shale wafers, white circle indicates the presence of visible inorganic veins on the sample surface.

Figure 2 shows the results of calibrated SANS measurements of the absolute value of the scattering intensity; two-dimensional scattering patterns (not shown) were isotropic and the azimuthally averaged SANS intensity profiles appear on the log-log scale to be uniform (Figure 2a). Figure 2b shows the relative SANS intensity calculated for each wafer, normalised to the wafer-average intensity at each fixed Q-value; the largest departures from the average are observed for the thicker wafers L5 and L8 (Table B1). The vertically expanded view presented in Figure 2c indicates that in most of the SANS Q-range the relative scattering intensity varies within the limits of about ±15% with the largest variation of ~20% for wafer L8 in the large-Q region (Table B1).

Variation observed in the large-Q SANS region (Figure 2c) may be caused by the incoherent scattering on various amounts of hydrogen present in the remnant water and (or) moisture bound in the pores, the fingerprints accidentally left on the sample surface and the water bound in smectite (abundant in New Albany Shale; see Supplementary Material Table A1). In addition, propagated measurement statistical errors also contribute to the variation, (section 4.2). Fluctuations of the relative intensity in the SANS small-Q range observed for the thickest wafers (L5, L6, L8 and L9; Figure 2c and Table B1) may be indicative of the onset of multiple scattering (MS) effects (Ji et al. 2022). Also, wafers L5, L8 and L9 have discoloured stripes visible on both surfaces (Figure 1) due to inorganic veins (possibly quartz or calcite) that may affect the volume-average microstructure and, consequently, enhance the departure of SANS intensity from the average.

It is evident that the departure from the average SANS profile is most likely caused by the heterogeneity of the rock fabric on the centimetre scale and/or details of the preparation and handling procedures. The former provides useful information on its own under various investigations of the shale, while the latter should be eliminated at the sample preparation and handling stage to minimise the experimental errors, which is also one of the main purposes of this study. In this study we do not consider the effect of mineralogical variation on the variability of scattering data. Earlier studies (Bahadur et al. 2018) have shown that mineralogical changes do not significantly affect SANS result. Their effect becomes only apparent when performing contrast matching experiments, which reveal that mineralogical changes influence accessibility of fluids to the pore space.

For the reduction of sample variability sets of wafers were selected with minimum geometrical artefacts by discarding those with physical imperfection (e.g., scratches, cracks and removable residues on the sample surface) or potentially susceptible to the MS effects

(L5, L6, L8 and L9 for this wafer set); SANS results for the selected "artefact reduced" subset of wafers are shown in Figure 2d. Thicknesses of these wafers are similar, ranging from 0.68 to 0.81 mm (Table 4). Compared to the SANS results for the full set of wafers (Figure 2c) there is much less relative intensity variation between the samples (Figure 2d), in general reduced from around ±15% to ±10% (see details in Table B1).

SANS results presented in Figure 2 (a-c) illustrate the degree of the rock core inhomogeneity on the centimetre scale. The investigation aims to additionally provide a baseline for the selection of multiple sets by a careful visual inspection (here called further on "artefact reduced") used in laboratory-controlled destructive physical or chemical environments. For instance, for a representative study of a homogeneous sub-volume of the rock core, samples which contain visible physical imperfections or the excessively thick wafers (potentially susceptible to MS effects) should be identified and removed at the sample selection stage, inorganic veins or other inherent heterogeneities should be identified and carefully considered prior to measurements. If this is not possible or impractical, the potentially problematic samples should be used with experimental or interpretative modifications, such as a choice of a smaller beam diameter, application of MS treatment techniques (Jaksch et al. 2021), or selection of a MS-minimised Q-range (Ji et al. 2022).

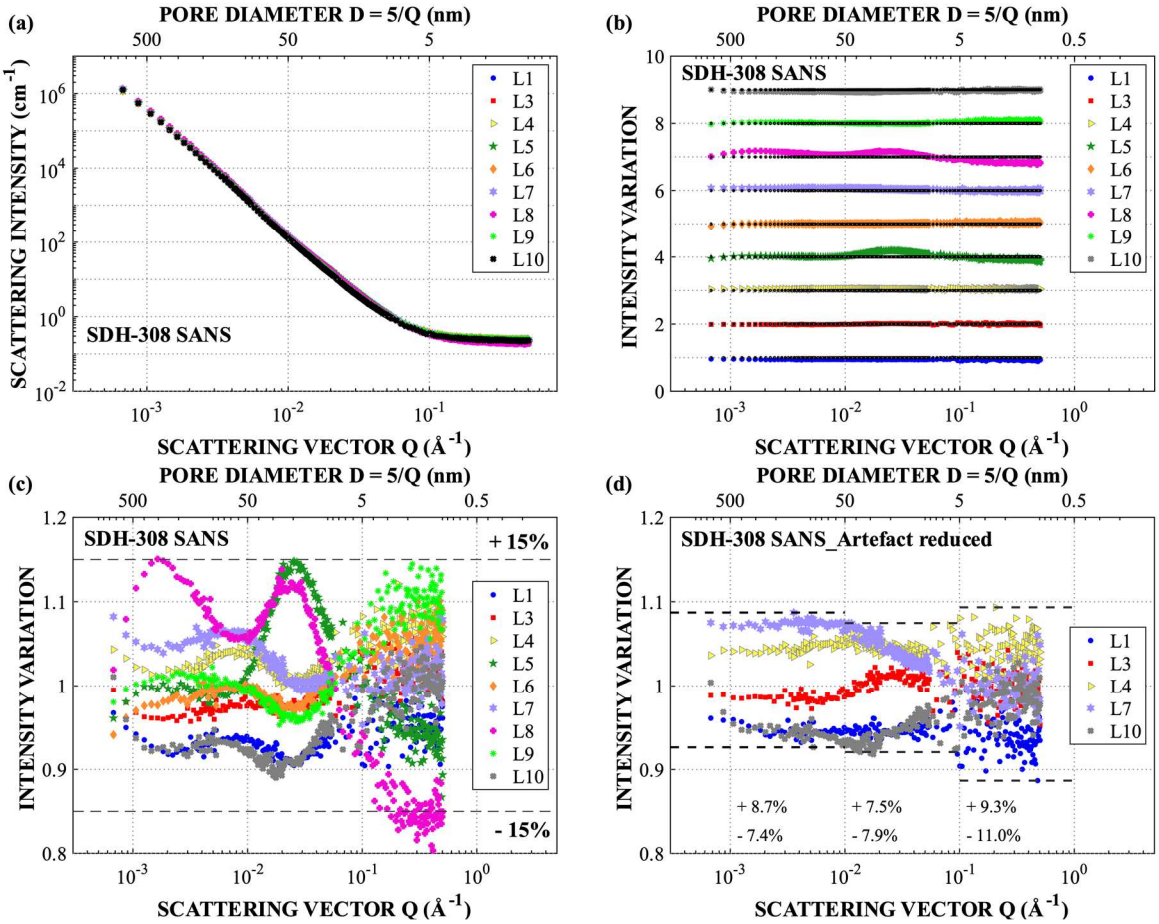

Figure 2. SANS intensity results for SDH-308 shale wafers: (a) SANS scattering intensity profile for nine shale wafers; (b) relative scattering intensity variation for each wafer (the intensity profile for each wafer is shifted up for clarity); Magnification of the relative scattering intensity variation for (c) nine wafers and (d) the artefact reduced data set; the numbers above the x-axis indicate the general variation range for each Q range.

4.1.2 SANS and USANS results for McAtee-2798 wafers

McAtee-2798 wafers were cut from a mid-mature New Albany Shale core from Pike Country, Indiana (the sample depth 852.8 m), which contained medium thermal maturity organic matter (TOC = 6.6 weight %, R_o = 0.7%; Table 1). In total, five wafers with similar thicknesses (0.79-0.83mm) were measured using SANS and three using USANS (Table 2). The physical appearance of the two faces parallel to the bedding plane for each sample is illustrated in Figure A1 (Supplementary Material A); the azimuthally averaged SANS and desmeared USANS intensity profiles are presented in Figure 3a and Figure 4 (a, b), respectively.

The desmearing processing of USANS data may artificially magnify and introduce random errors (Jackson et al. 2008, Ji et al. 2022). Thus, this study focuses on the original smeared data in the analysis of intensity variations. Furthermore, as the instrument does not

collect the scattered intensity at precisely the same Q value at consecutive scans, the interpolation written in the Python scripts is used for USANS (Kookaburra) data processing (Arnold et al. 2014) to achieve direct comparison. The result with error bars is reported in Figure B5.

Figure 3a demonstrates that SANS intensity profiles on the log-log scale are uniform in most of the SANS Q-range, with the exception of the wafer L2 in the large-Q region (deviation by up to around 40%; Figure 3b). For other wafers, the variation of relative scattering intensity stays within the limits of about ±10% in most of the SANS Q-range (Figure 3 and Table B2). The "selected" subset excludes wafer L2 (because of the deviation described above) and wafer L6 (which may be subject to MS, as shown in the small-Q region in Figure 3b), which have also been used for USANS measurements; SANS intensity variation in most of Q-range is below ±5% and around ±10% in the large-Q region (Figure 3c). The causes of the outlying SANS results for wafer L2 are not clear as its physical appearance is uniform (Figure A1).

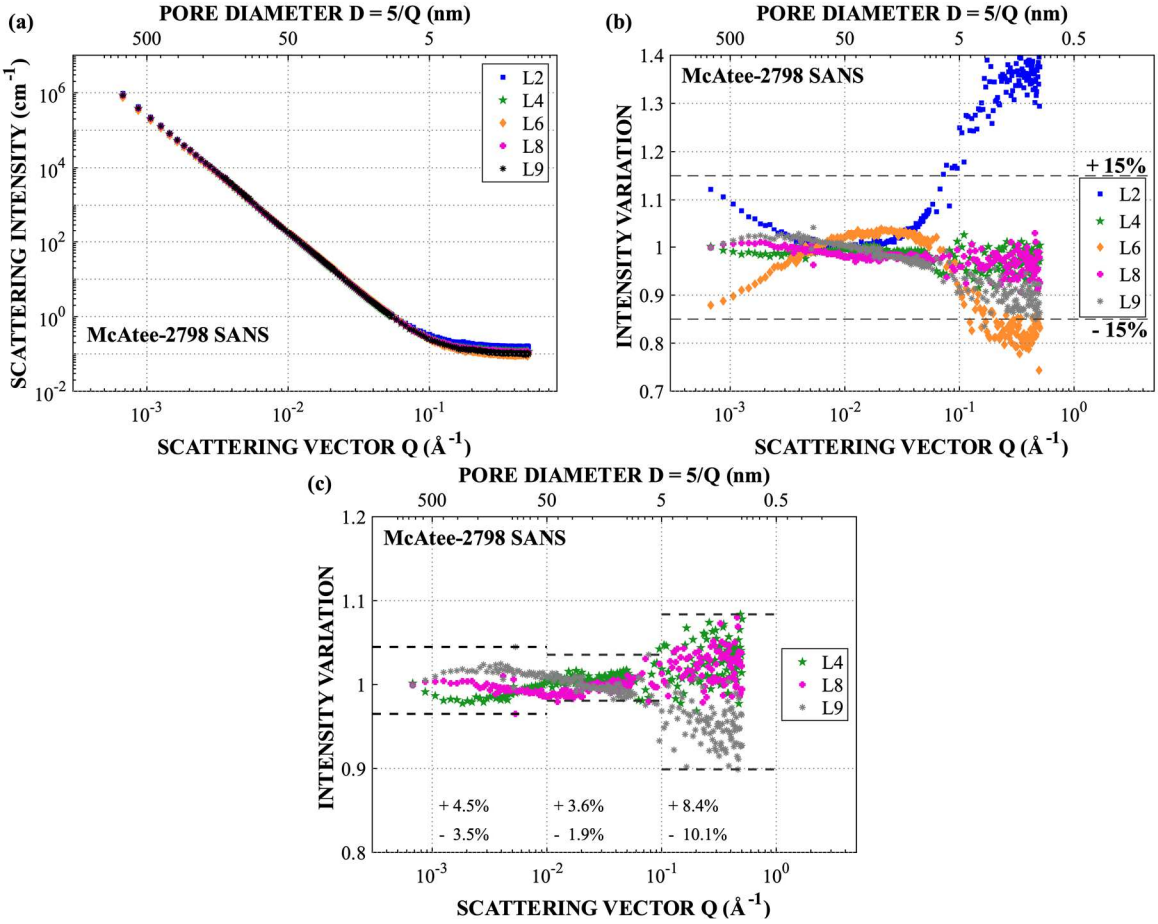

Figure 3. SANS intensity results for McAtee-2798 shale wafers: (a) SANS scattering intensity profile for five shale wafers. Magnification of the relative scattering intensity

variation for (b) five shale wafers and (c) three selected wafers (further measured in the USANS).

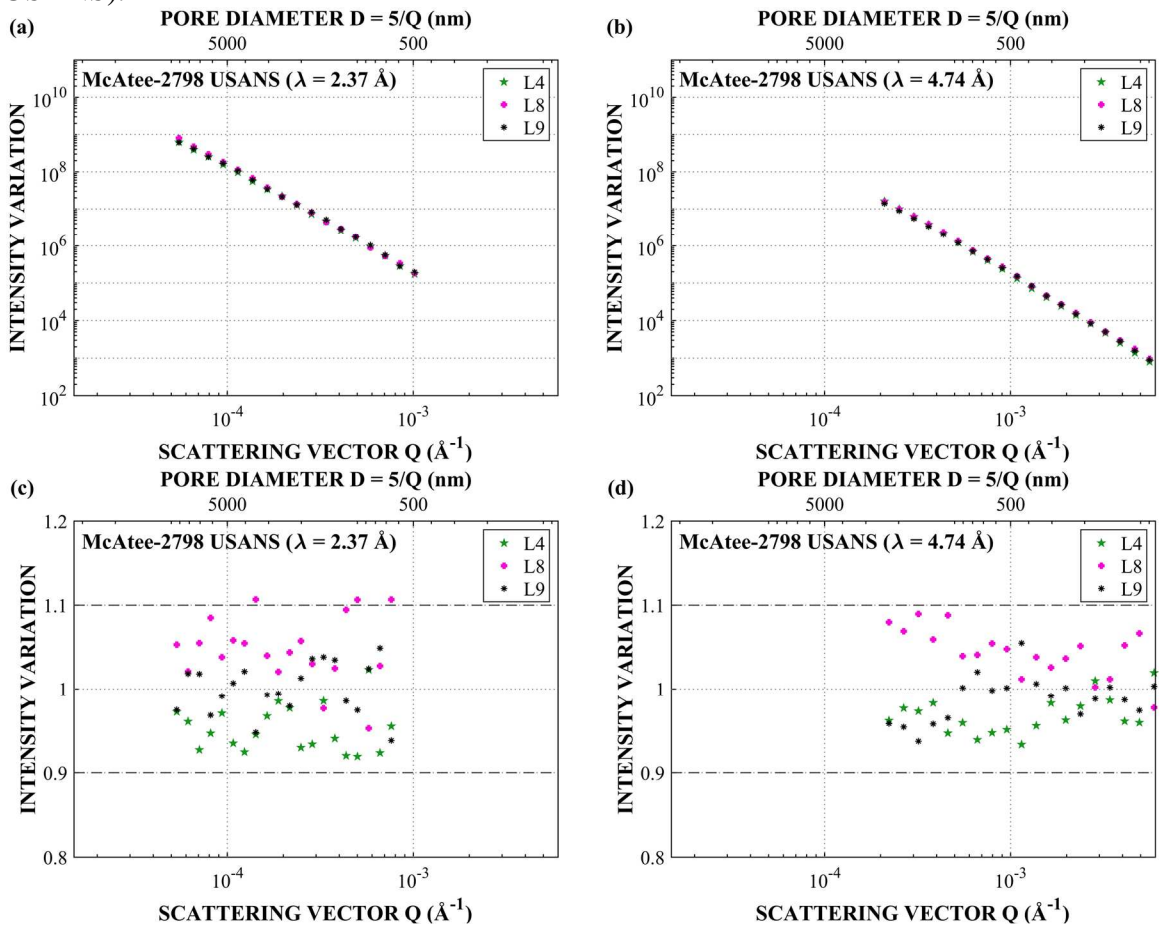

Figure 4. USANS scattering results for three McAtee-2798 shale wafers: MS-minimised absolute scattering intensity profile (desmeared) at (a) λ = 2.37 Å and (b) λ = 4.74 Å. Magnification of the relative USANS scattering intensity (smeared) variation for measurement at (c) λ = 2.37 Å and (d) λ = 4.74 Å. Results including error bars (uncertainties) caused by the counting statistics and experimental procedures are shown in Figure B5, Supplementary Material B.

Figure 4 shows the MS-minimised results (the distorted intensity affected by MS effects at the USANS small Q-region has been excluded) based on the recent MS study (Ji et al. 2022). Figure 4a and Figure 4b indicate the uniformity of the scattering intensities of three McAtee-2798 shale wafers with around ±10% variation in the USANS Q region (measured using λ = 2.37 Å and 4.74 Å, respectively). In general, the variation of relative USANS intensity measured using λ = 2.37 Å is slightly larger for λ = 4.74 Å (Figure 4 (c, d)), and about twice the relative intensity in most of the SANS Q-range (Figure 3c). Plots of the relative USANS intensity with error bars are shown in Figure B5 (Supplementary Material).

A more quantitative analysis for the standard deviation of the overall scattering intensity variation and statistical errors of the measurements is included in Supplementary Material Table B8 and Table B9. This shows that in the SANS range, the statistical errors (1

sigma) are on the order of 2%, and the overall scattering intensity variation is 3% to 22%, demonstrating that the sample variation is dominating the overall variation. In the USANS range, on the other hand, the data shows that the overall variation (3-7%) is comparable to the statistical errors (4-6%), demonstrating that both the measurement uncertainty (statistical errors) and sample variation significantly contribute to the observed overall variation.

Detailed results and interpretation for cores Gibson-3997, Hardin-IL2, Hardin-IL3 and Marcellus-7084 are provided in Supplementary Material B.

348 4.1.3 USANS instrumental reproducibility

349 The use of precisely oriented perfect crystals of Si in the design of USANS
350 instruments makes experimental results very sensitive to small fluctuations of the ambient
351 temperature (due to thermal expansion) and remnant mechanical strain which may cause
352 deformation of the elements of the neutron optics (Agamalian et al. 1997). These issues are
353 not entirely eliminated by the careful design of modern USANS instruments, as evidenced by
354 the need to compensate for the often-occurring shift of the maximum of the rocking curve
355 Bragg peak between consecutive experimental runs (note that the measured angles and angle
356 increments are very small; as an example, the direct beam in the short wavelength
357 configuration has a full width at half maximum of 3×10^{-4} degrees, and the full measurement
358 typically spans 0.03 degrees). This inherent instrumental instability may affect the
359 reproducibility of USANS results. To quantify this aspect of the experimental procedure,
360 USANS measurements (using $\lambda = 2.37$ Å) were conducted for two wafers: Gibson-3997 L8
361 and Marcellus-7084 L10 (a fresh wafer with the thickness of 0.7 mm, cut from the same
362 Marcellus core). Wafer L8 has been scanned in two consecutive one-hour runs over a limited
363 Q-range and wafer L10 has been consecutively measured using eight acquisition times (from
364 3 hours to 14 hours; Table 3). Two measurements improved counting statistics (2000 instead
365 of 1000 target counts per data point), resulting in a reduced statistical error (1-sigma) in the
366 measured data from 3% to 2%, and the other measurements were varied over the number of
367 points and point spacing (Table 3). Particular choice of acquisition time usually is a
368 compromise between the statistical error (count accuracy) and the amount of the available
369 beam time; statistical error (standard deviation) for a Poisson process is the square root of the
370 number of counts (Pomme et al. 2015); for instance, the rate of 1000 counts per a single Q-
371 value routinely used in this work corresponds to a 3% statistical error. Alternatively, it is
372 possible to trade data density for improved accuracy and reduce the number of data points per
373 run (especially the Q-points with low scattering intensity, which require a long acquisition
374 time).

375 Figure 5a shows that for sample L8 (Gibson-3997) the instrumental reproducibility of
376 USANS intensity is better than ±4%. However, this 4% variation is mainly contributed by the
377 measurement statistical error (Table B10). Figure 5b shows that for the eight measurements
378 performed on the Marcellus-7084 L10 wafer, the instrumental reproducibility is better than
379 ±5%, (and a little higher at high Q-range, where counting statistics degrade). A statistical
380 analysis shows that the standard deviation of the observed variation for both samples (2-5%)

lies well within the standard deviation of the statistical errors (3-5%) (Table B10). This demonstrates that the observed variability can be attributed in all cases to the counting statistics, and that there is no additional instrument contribution detected.

Table 3. Acquisition times for Gibson-3997 L8 and Marcellus-7084 L10 measured in the USANS (λ = 2.37 Å).

Sample name	Run name	Acquisition time (hours)	Counts	Maximal time	Points	Step size	Limited high Q
Gibson-3997 L8	L8_1	1	1000	1200	16	15	2.2E-04
	L8_2	1	1000	1200	16	15	2.2E-04
Marcellus-7084 L10	14	14	2000	2400	40	10	1.2E-03
	7.5_1	7.5	1000	1200	40	10	1.2E-03
	5	5	1000	1200	27	15	1.2E-03
	4	4	1000	1200	22	18	1.1E-03
	3.5	3.5	1000	1200	19	20	9.0E-04
	3	3	1000	1200	19	25	9.0E-04
	6.5	6.5	2000	2400	19	20	9.0E-04
	7.5_2	7.5	1000	1200	40	10	1.2E-03

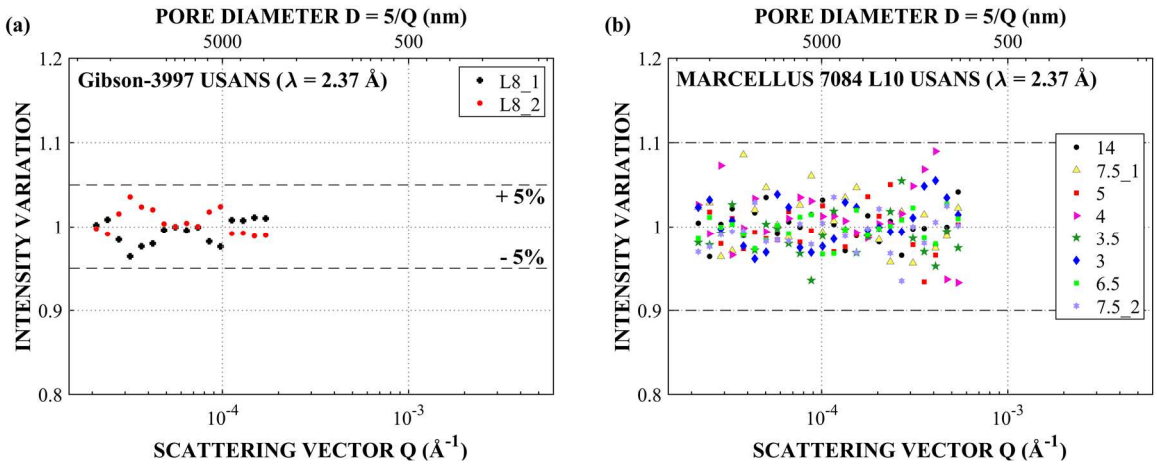

Figure 5. Magnification of the USANS relative scattering intensity variation results used to quantify instrumental stability: (a) two consecutive measurements for wafer Gibson-3997 L8; (b) wafer Marcellus-7084 L10 measured using eight different acquisition times.

391 **4.2 Summary of SANS and USANS results for six shale cores**

392 This study has examined the uniformity of the SANS (pore size range from 2 nm to
393 700 nm) and USANS (pore size range from 200 nm to 20 μm) scattering intensity for a
394 number of sub-millimetre thick wafers cut from about 1 cm long oriented core intervals from
395 unconventional shales of varying thermal maturity, obtained from five locations in the New
396 Albany Shale and the Marcellus Shale Formations in North America: six sets of consecutive
397 shale wafers measured using SANS and five sets measured using USANS.

398 Scattering intensity at a fixed scattering angle (represented by a Q-value) is proportional to
399 the concentration of pores of the radius about 2.5/Q (Equation 3) and, therefore, is a proxy for
400 the spatial uniformity of the fractional porosity on the centimetre scale. Due to the limited
401 beam time allocated, for most samples the USANS acquisition time has been optimised and
402 the low scattering datapoints at the high Q-end have not been measured. Therefore, these
403 results demonstrate a general similarity of the USANS scattering intensity in the limited Q-
404 range only ($Q<2\times10^{-4}$ $Å^{-1}$), hence the SANS and USANS data do not overlap and are
405 discussed separately. In general, the measured intensity variation with the pore size (relative
406 to the average) is about ±15% in most of the SANS Q-range and about ±20% in the large Q-
407 region (pore size < 5 nm) for the majority of studied wafers (Figure 3b). In general, most of
408 the variation in the SANS Q-range is contributed by microstructural heterogeneity of the rock
409 core (Li et al. 2017). However, in the USANS Q-region and large-Q SANS region ($Q>1\times10^{-1}$
410 $Å^{-1}$) for some rocks, the observed variations are dominated by both the measurement
411 statistical errors and the rock heterogeneity (See Supplementary Material Table B8 and Table
412 B9). Factors that contribute to the centimetre-scale spatial fluctuation of SANS intensity
413 along the core (discussed in detail in sections 4.1 and listed in Tables 4 and 5) are as follows:

414 1. Physical imperfection and (or) inherent heterogeneities in the rock matrix.
415 2. Multiple scattering effects in the SANS small-Q region for relatively thicker
416 wafers.
417 3. Alteration of the near-surface pore structure due to the invasive sample
418 preparation and handling procedure.
419 4. Incoherent scattering from hydrogen nuclei presents in water (moisture),
420 bound water (smectite) and organic matter hosted in the pore space (dominant
421 in the SANS large-Q region).
422 5. Experimental and data processing factors: statistical errors caused by the
423 counting protocols (about 1.5% in SANS low-Q data, 2.5% in SANS high-Q

data and 4.0 - 6.0% for USANS data) and imprecise data match between various SANS configurations.

6. Importantly, USANS measurements are highly reproducible and coincide within the experimental uncertainty stemming from the counting statistics (typically 3%).

In most of the SANS Q-region, there is an approximate correlation between the relative scattering intensity variation and the thermal maturity (quantified by R_o; Table 1): the lower the thermal maturity of the shale, the greater the intensity variation in most of the SANS Q-range (with the exception of the post-mature Hardin-IL3 core, extracted from an outcrop; Figure 6a). Moreover, a positive correlation between the relative intensity variation results and the sample scattering power (defined as $\tau = -\ln(T_{SAS})$, Ji et al. (2022)) is revealed using the experimentally determined USANS T_{SAS} values ($\lambda = 2.37$ Å) for wafers from different cores with similar thicknesses (Supplementary Material; Table B11; Figure 6b). Note that T_{SAS} is the small angle scattering transmission, which reflects the total porosity of shale wafers (i.e., the larger total porosity, the larger scattering power (Ji et al. 2022). There is no apparent correlation between the intensity variation and the total organic carbon (TOC) (Figure 6c).

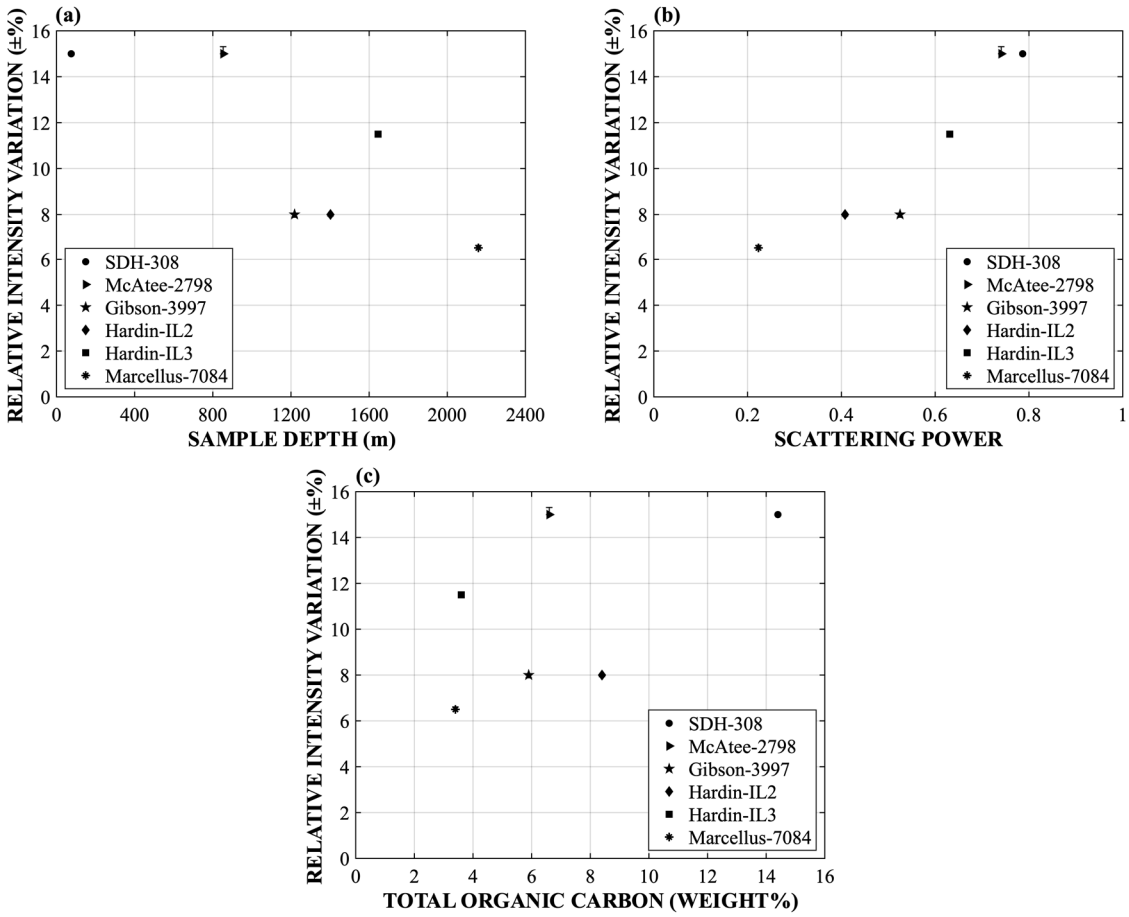

441

442 Figure 6. The correlation between the relative intensity variation in most of SANS Q-range
443 and (a) the sample depth; (b) scattering power; (c) total organic carbon (TOC, weight %).
444

445 Table 4. Summarised relative intensity variation in various Q-ranges for six sets of shale
446 wafers measured using SANS.

Sample name		Number of wafers	Thickness range (mm)	Relative intensity variation (%)		
				Q<1E-2	1E-2<Q<1E-1	Q>1E-1
SDH -308	Original	9	0.68 - 0.92	±15	±15	±20
	Artefact reduced	5	0.68 - 0.81	±9	±8	±11
McAtee -2798	Original	5	0.79 - 0.83	±12	±15	±40
	Selected*	3	0.79	±5	±4	±10
Gibson -3997	Original	8	0.81 - 0.94	±7	±8	±14
	Artefact reduced	5	0.81 - 0.90	±5	±7	±14
	Selected*	3	0.84 - 0.90	±4	±5	±8
Hardin -IL2	Original	8	0.57 - 0.83	±6	±8	±16
	Selected*	3	0.79 - 0.80	±4	±7	±11
Hardin -IL3	Original	8	0.76 - 0.87	±9	±12	±22
	Selected*	3	0.79 - 0.82	±4	±8	±18
Marcellus -7084	Original/USANS	5	0.22 - 1.00	±6	±7	±15

447 * See also USANS result (Table 5).

448 Table 5. Relative intensity variation for five sets of shale wafers measured using USANS.

Sample name	Number of wafers	Thickness range (mm)	USANS Relative intensity variation (%)	
			λ = 2.37 Å	λ= 4.74 Å
McAtee-2798	3	0.79	±10	±9
Gibson-3997	3	0.84 - 0.90	±5	no data
Hardin-IL2	3	0.79 - 0.80	±9	no data
Hardin-IL3	3	0.79 - 0.82	±8	no data
Marcellus-7084	5	0.22 - 1.00	±13	±14

449

450 **4.3 Spatial variation of the pore size distribution on the centimetre scale in the**
451 **Marcellus-7084 core**

452 Spatial variation of the pore structure in the studied shale cores has been examined
453 using the fits of joined SANS-USANS results to the PDSP numerical model coded in the
454 PRINSAS software (which assumes spherical pore shapes; (Hinde 2004)).

455 Figure 7 (a, b) illustrates the MS-minimised USANS and SANS combined scattering
456 intensity and relative intensity plots for five Marcellus-7084 shale wafers, respectively
457 (detailed SANS and USANS results are presented in section B4). The combined scattering
458 intensity plots appear very uniform; the shaded regions (grey, yellow and green) mark the
459 fluctuation results in the USANS Q-range, most of the SANS Q-range and the SANS large Q-
460 region, respectively. The result calculated for the combined scattering intensity is of a similar
461 or slightly larger magnitude than fluctuations of the separate USANS and SANS scattering
462 intensity (Figure 7b and Figure B4). Figure 7(c, d) shows PRINSAS-determined results; on
463 the log-log scale the probability density distributions for pore sizes, f(r), the specific surface
464 areas measured by different probe sizes, SSA(R), and the incremental pore volumes, dV/dr,
465 appear very similar, even though small discrepancies occur for several Q-values in both
466 SANS and USANS Q-regions. Fluctuations of the incremental pore volume, dV/dr, appear to
467 be most evident in the USANS Q-region (Figure 7d). The PRINSAS-determined porosities,
468 average pore volumes, pore concentrations and their variability, which were calculated using
469 the combined SANS-USANS data for each wafer, are compiled in Table 6.

470 Results listed in Table 4 (spatial variation of SANS intensity), Table 5 (spatial
471 variation of USANS intensity) and Table 6 (spatial variation of the porosity, average pore
472 size and pore concentration) indicate that the spatial variation of PRINSAS-determined
473 microstructural properties is of the same order as the variation of the scattering intensity in
474 the most of the SANS Q-range (about ±9%, Figure 7b). The relative variation of PRINSAS-

475 determined microstructural parameters has also been determined for SANS data obtained for
476 the five artefact-reduced SDH-308 wafers, SANS-USANS combined data for three selected
477 wafers of McAtee-2798, Gibson-3997, Hardin-IL2 and Hardin-IL3; the results are close to
478 the relative SANS intensity variation (Table 4 and Table 7). However, using the Q-limited
479 USANS scans for Gibson-3997, Hardin-IL2 and Hardin-IL3 wafer sets may not accurately
480 estimate the microstructural properties, because the Q-range of data gap between two
481 scattering methods (e.g., USANS and TOF-SANS) requires significant extrapolation and
482 interpolation of the SANS small-Q or the USANS large-Q region, which may create artefacts.
483 In general, the cores hosting immature to the mid-mature organic matter have more variable
484 SANS intensity and larger total porosity than the late to post-mature shales (Mastalerz et al.
485 2018). However, this conclusion may be affected by the selection of two under-determined
486 parameters used in PRINSAS computations: the experimentally estimated value of the SANS
487 large-Q background and the scattering length density (SLD) of TOC for each shale; in the
488 absence of detailed chemical analysis of the organic matter for the New Albany Shale cores,
489 the SLD of the organic matter component has been approximated by analogy with coals of
490 similar thermal maturity (Radlinski et al. 2004). In addition, we assumed the nominal specific
491 density of the mineral rock matrix components.

492 Table 6. PRINSAS-determined porosity, average pore volume, and pore concentration using
493 MS-minimised SANS-USANS combined scattering intensity for five Marcellus-7084 wafers.
494 The variation of pore properties calculated for each wafer is normalised to the wafer-average
495 property value.

Sample name	PRINSAS-determined pore properties (SANS+USANS)					
	Porosity (%)	Variation (%)	Average Pore Volume (cm^3)	Variation (%)	Pore Concentration (cm^{-3})	Variation (%)
Lh	4.5	-3.1	1.26E-19	2.8	3.58E+17	-6.0
Lf	4.7	1.5	1.32E-19	8.4	3.56E+17	-6.6
Le	4.7	0.2	1.18E-19	-3.4	3.94E+17	3.4
Ld	4.8	3.4	1.20E-19	-1.8	4.00E+17	5.1
Lc	4.5	-2.1	1.15E-19	-6.1	3.96E+17	4.0

496

497 Table 7. The averaged PRINSAS-determined pore properties and related variation using
498 SANS intensity of SDH-308 wafers, SANS-USANS combined intensity of McAtee-2798,
499 Gibson-3997, Hardin-IL2, Hardin-IL3 and Marcellus-7084 wafers. Note: symbol * makes
500 wafers measured using USANS Q-limited scan.

Sample name	Wafer number	Averaged PRINSAS-determined pore properties						
		Porosity (%)	Variation (%)	Average Pore Volume (cm^3)	Variation (%)	Pore Concentration (cm^{-3})	Variation (%)	Instrument
SDH-308	5	5.1%	±6	2.00E-19	±5	2.56E+17	±8	SANS
McAtee-2798	3	7.5%	±1	7.09E-20	±4	1.05E+18	±5	SANS + USANS
*Gibson-3997	3	9.4%	±3	7.98E-20	±6	1.18E+18	±4	SANS + USANS
*Hardin-IL2	3	4.7%	±1	2.08E-19	±6	2.26E+17	±6	SANS + USANS
*Hardin-IL3	3	4.8%	±3	3.63E-19	±4	1.33E+17	±7	SANS + USANS
Marcellus-7084	5	4.6%	±3	1.22E-19	±8	3.81E+17	±7	SANS + USANS

501

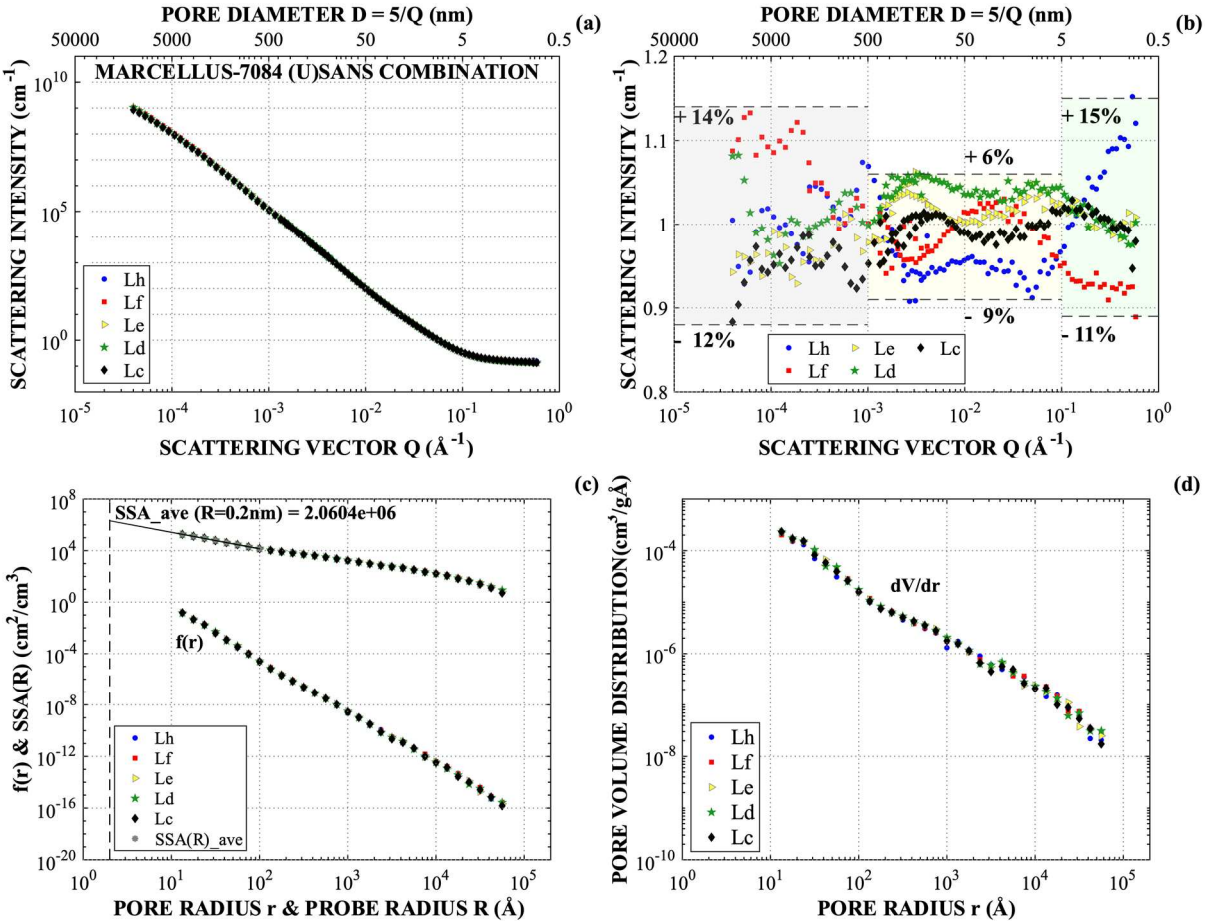

Figure 7. MS-minimised SANS-USANS combined results for five Marcellus-7084 wafers: (a) scattering intensity; (b) magnification of relative scattering intensity variation; PRINSAS-determined microstructural properties: (c) f(r) and SSA(R); (d) dV/dr.

5. Conclusion and Recommendations

SANS and USANS measurements have been performed on six American unconventional shale cores. Tests for intensity uniformity and volume-representativity of consecutive submillimetre wafers sliced in the direction of the sedimentation plane were performed. For each core, the SANS and USANS intensity results for the corresponding set of slices remain within the range of ±15% from the average for most of the Q-range, and the fluctuation can be reduced to less than ±10% by a careful sample preparation and data processing (e.g., using artefact reduced wafer sets (Table 4)). We consider this number as a measure of the statistical equivalence of individual slices, which is controlled by the centimetre-scale homogeneity of the core pore structure (for pore sizes extending from ~1 nm to 20 μm) and the rock matrix chemical composition of consecutive wafers (with a spatial resolution of below 1mm). In other words, the fluctuation of SANS and USANS intensity determines to what degree each wafer can be considered a representative sub-sample (representative volume) of the core.

There are several factors that may cause the scatter of experimental results from slice to slice, including the inherent heterogeneities (e.g., inorganic veins), physical imperfections of wafers (e.g., regions of damage and residues left on the wafer due to sample preparation and handling), multiple scattering (MS) effects for relatively thick wafers, possible near-surface pore structure damage caused by preparing overly thin wafers, and the incoherent scattering from hydrogen atoms present in the bound water and the organic matter, which may cause a relatively large variation in the SANS large-Q range (for $Q \geq 0.1$ Å^{-1}). Additional artefacts may be caused by experimental statistical errors (generally larger in the SANS large-Q range and the USANS Q-range), imprecise data matching between the SANS and USANS Q regions and (or) various SANS configurations, experimental noise, and instrumental reproducibility (typically ±3%). For the core material studied here, the statistics of the scattering intensity uniformity (obtained by comparing the relative intensity of each wafer) can be improved by up to ±7% when the above problems have been eliminated; this emphasizes the importance of careful sample preparation, sample selection and data processing procedures before and during SAS studies, especially when multiple samples are used. For all cores studied in this work, the spatial (wafer-to-wafer) variation of microstructural properties (determined by fits to the microstructural PRINSAS polydisperse spheres model), including the total porosity, averaged pore volume and pore concentration, is reflecting the relative variation of the corresponding scattering intensity; therefore, the

relative intensity of the SANS and USANS intensity is a reasonable proxy for the relative variation of the microstructural parameters.

Results of SANS measurements reveal an approximate correlation between the intensity variation and thermal maturity of the organic matter (Figure 6a), as well as a strong positive correlation between the relative intensity variation (in most of the SANS Q-range) and the scattering power, τ, of shale (Figure 6b). The value of τ has been estimated from measurements of T_{SAS} for wafers from each sample set in the USANS Q-region (using λ = 2.37 Å; Table B10). The intensity variation - τ correlation could not be reliably tested in the USANS Q-range due to the small number of samples studied using USANS. No correlation is apparent between the intensity variation and TOC (Fig. 6c).

A potentially worrying result is the large (up to 18%) relative intensity variation of consecutive wafers in the SANS large-Q region (Table 4) and the USANS Q-region (Table 5), which suggests that representative samples may not be reliably selected from adjacent wafers due to excessive variability. However, the variability of pore properties calculated from these results is partially compensated and reduced to less than ±10 % (Table 7). It is concluded that selection of representative samples by using consecutive wafers is a robust approach for the purpose of microstructural studies.

In general, the scattering intensity variation between consecutive wafers decreases from the USANS Q-range (measured using λ = 2.37 Å) to the SANS mid-Q range (i.e., for $Q<0.1$ Å^{-1}); the maximal variation is observed in the SANS large-Q region. It is evident that larger variations of the scattering intensity (and, consequently, total porosity) occur in cores hosting less mature organic matter. The robustness of this observation is evidently affected by the methodology of sample selection, data interpretation and instrument-specific reproducibility.

To conclude, for the cores of the New Albany Shale and the Marcellus Shale studied here, the SANS and USANS data acquired from appropriately selected submillimetre wafers are volume-representative for the about one-centimetre-deep core material with an error of less than ±10%.

Acknowledgements

This research was supported by a fellowship from the UNSW Tuition Fee Scholarship (TFS), the China Scholarship Council (CSC) and an AINSE Ltd, Postgraduate Research Award (PGRA). The sample material was supplied by Maria Mastalerz from the University

of Indiana, based upon work supported by the U.S. Department of Energy, Office of Science, Office of Basic Energy Sciences, Chemical Sciences, Geosciences, and Biosciences Division under Award Number DE-SC0006978. This work was supported by the Australian Nuclear Science and Technology Organization in providing the SANS and USANS neutron research facilities (Proposals: P8360, P8325, P9059 and P9616) used in this work. Furthermore, we also acknowledge support from the Australian Research Council (ARC DP170104550, DP170104557, LP170100233 and LE200100209).

References

Agamalian, M, GD Wignall and R Triolo (1997). "Optimization of a Bonse–Hart ultra-small-angle neutron scattering facility by elimination of the rocking-curve wings." Journal of Applied Crystallography **30**(3): 345-352.

Allen, AJ (1991). "Time-resolved phenomena in cements, clays and porous rocks." Journal of Applied Crystallography **24**(5): 624-634.

Altman, Douglas G and J Martin Bland (2005). "Standard deviations and standard errors." Bmj **331**(7521): 903.

Anovitz, Lawrence M and David R Cole (2015). "Characterization and analysis of porosity and pore structures." Reviews in Mineralogy and Geochemistry **80**(1): 61-164.

Anovitz, Lawrence M, Gary W Lynn, David R Cole, Gernot Rother, Lawrence F Allard, William A Hamilton, Lionel Porcar and Man-Ho Kim (2009). "A new approach to quantification of metamorphism using ultra-small and small angle neutron scattering." Geochimica et Cosmochimica Acta **73**(24): 7303-7324.

Arnold, Owen, Jean-Christophe Bilheux, JM Borreguero, Alex Buts, Stuart I Campbell, L Chapon, Mathieu Doucet, N Draper, R Ferraz Leal and MA Gigg (2014). "Mantid—Data analysis and visualization package for neutron scattering and μ SR experiments." Nuclear Instruments and Methods in Physics Research Section A: Accelerators, Spectrometers, Detectors and Associated Equipment **764**: 156-166.

Bahadur, Jitendra, Cristian R Medina, Lilin He, Yuri B Melnichenko, John A Rupp, Tomasz P Blach and David FR Mildner (2016). "Determination of closed porosity in rocks by small-angle neutron scattering." Journal of Applied Crystallography **49**(6): 2021-2030.

Bahadur, Jitendra, Andrzej P Radlinski, Yuri B Melnichenko, Maria Mastalerz and Arndt Schimmelmann (2015). "Small-angle and ultrasmall-angle neutron scattering (SANS/USANS) study of New Albany Shale: a treatise on microporosity." Energy & Fuels **29**(2): 567-576.

Bahadur, Jitendra, Leslie F Ruppert, Vitaliy Pipich, Richard Sakurovs and Yuri B Melnichenko (2018). "Porosity of the Marcellus Shale: A contrast matching small-angle neutron scattering study." International Journal of Coal Geology **188**: 156-164.

Bale, Harold D and Paul W Schmidt (1984). "Small-angle X-ray-scattering investigation of submicroscopic porosity with fractal properties." Physical Review Letters **53**(6): 596.

Blach, Tomas, Andrzej P Radlinski, Dianne S Edwards, Christopher J Boreham and Elliot P Gilbert (2020). "Pore anisotropy in unconventional hydrocarbon source rocks: A small-angle neutron scattering (SANS) study on the Arthur Creek Formation, Georgina Basin, Australia." International Journal of Coal Geology: 103495.

Blach, Tomasz, Andrzej P Radlinski, Phung Vu, Yeping Ji, Liliana de Campo, Elliot P Gilbert, Klaus Regenauer-Lieb and Maria Mastalerz (2021). "Accessibility of Pores to Methane in New Albany Shale Samples of Varying Maturity Determined Using SANS and USANS." Energies **14**(24): 8438.

Blach, Tomasz, Andrzej P Radlinski, Phung Vu, Yeping Ji, Liliana de Campo, Elliot P Gilbert, Klaus Regenauer-Lieb and Maria Mastalerz (2021). "Deformation of pores in response to uniaxial and hydrostatic stress cycling in Marcellus Shale: Implications for gas recovery." International Journal of Coal Geology **248**: 103867.

Bowers, Geoffrey M., H. Todd Schaef, Quin R. S. Miller, Eric D. Walter, Sarah D. Burton, David W. Hoyt, Jake A. Horner, John S. Loring, B. Peter McGrail and R. James Kirkpatrick (2019). "13C Nuclear Magnetic Resonance Spectroscopy of Methane and Carbon Dioxide in a Natural Shale." ACS Earth and Space Chemistry **3**(3): 324-328.

Cao, Peng, Jishan Liu and Yee-Kwong Leong (2017). "A multiscale-multiphase simulation model for the evaluation of shale gas recovery coupled the effect of water flowback." Fuel **199**: 191-205.

Chen, Xiao, Hamid Roshan, Adelina Lv, Manman Hu and Klaus Regenauer-Lieb (2020). "The dynamic evolution of compaction bands in highly porous carbonates: the role of local heterogeneity for nucleation and propagation." Progress in Earth and Planetary Science **7**(1): 28.

Chiang, Wei-Shan, Daniel Georgi, Taner Yildirim, Jin-Hong Chen and Yun Liu (2018). "A non-invasive method to directly quantify surface heterogeneity of porous materials." Nature communications **9**(1): 1-7.

Clarkson, Christopher R, M Freeman, Lilin He, Michael Agamalian, YB Melnichenko, Maria Mastalerz, R Marc Bustin, AP Radliński and TP Blach (2012). "Characterization of tight gas reservoir pore structure using USANS/SANS and gas adsorption analysis." Fuel **95**: 371-385.

Clarkson, Christopher R, Nisael Solano, Robert M Bustin, AMM Bustin, Gareth RL Chalmers, Lilin He, Yuri B Melnichenko, AP Radliński and Tomasz P Blach (2013). "Pore structure characterization of North American shale gas reservoirs using USANS/SANS, gas adsorption, and mercury intrusion." Fuel **103**: 606-616.

Considine, Timothy J, Robert Watson and Seth Blumsack (2010). "The economic impacts of the Pennsylvania Marcellus shale natural gas play: an update." The Pennsylvania State University, Department of Energy and Mineral Engineering.

Espinat, D (1990). "Application des techniques de diffusion de la lumière des rayons X et des neutrons à l'étude des systèmes colloïdaux. Première partie: Présentation théorique des trois techniques." Revue de l'Institut français du pétrole **45**(6): 775-820.

Ge, Jiachao, Xiaozhou Zhang and Furqan Le-Hussain (2022). "Fines migration and mineral reactions as a mechanism for CO2 residual trapping during CO2 sequestration." Energy **239**: 122233.

Gilbert, Elliot P., Jamie C. Schulz and Terry J. Noakes (2006). "'Quokka'—the small-angle neutron scattering instrument at OPAL." Physica B: Condensed Matter **385-386**: 1180-1182.

Gu, Xin, David R Cole, Gernot Rother, David FR Mildner and Susan L Brantley (2015). "Pores in Marcellus shale: A neutron scattering and FIB-SEM study." Energy & Fuels **29**(3): 1295-1308.

Hinde, Alan L (2004). "PRINSAS–a Windows-based computer program for the processing and interpretation of small-angle scattering data tailored to the analysis of sedimentary rocks." Journal of Applied Crystallography **37**(6): 1020-1024.

Jackson, A, S Kline, J Barker and D Mildner (2008). "SANS and USANS Investigation of Oil Uptake by Micellar Gels."

Jaksch, Sebastian, Vitaliy Pipich and Henrich Frielinghaus (2021). "Multiple scattering and resolution effects in small-angle neutron scattering experiments calculated and corrected by the software package MuScatt." Journal of Applied Crystallography **54**(6).

Ji, Yeping, Andrzej P Radlinski, Tomasz Blach, Liliana de Campo, Phung Vu, Hamid Roshan and Klaus Regenauer-Lieb (2022). "How to avoid multiple scattering in strongly scattering SANS and USANS samples." Fuel **325**: 124957.

Kline, Steven R (2006). "Reduction and analysis of SANS and USANS data using IGOR Pro." Journal of Applied Crystallography **39**(6): 895-900.

Lee, Dae Sung, Jonathan D Herman, Derek Elsworth, Hyun Tae Kim and Hyun Suk Lee (2011). "A critical evaluation of unconventional gas recovery from the Marcellus Shale, northeastern United States." KSCE Journal of Civil Engineering **15**(4): 679-687.

Li, Lihui, Beixiu Huang, Yufang Tan, Xiaolong Deng, Yanyan Li and Hu Zheng (2017). "Geometric Heterogeneity of Continental Shale in the Yanchang Formation, Southern Ordos Basin, China." Scientific Reports **7**(1): 6006.

Liu, Jie and Klaus Regenauer-Lieb (2021). "Application of percolation theory to microtomography of rocks." Earth-Science Reviews **214**: 103519.

Liu, Kouqi, Mehdi Ostadhassan, Liangwei Sun, Jie Zou, Yujie Yuan, Thomas Gentzis, Yuxiang Zhang, Humberto Carvajal-Ortiz and Reza Rezaee (2019). "A comprehensive pore structure study of the Bakken Shale with SANS, N2 adsorption and mercury intrusion." Fuel **245**: 274-285.

Lucido, G, R Triolo and E Caponetti (1988). "Fractal approach in petrology: Small-angle neutron scattering experiments with volcanic rocks." Physical Review B **38**(13): 9031.

Mastalerz, Maria, Agnieszka Drobniak and Artur B. Stankiewicz (2018). "Origin, properties, and implications of solid bitumen in source-rock reservoirs: A review." International Journal of Coal Geology **195**: 14-36.

Melnichenko, YB, AP Radlinski, Maria Mastalerz, G Cheng and J Rupp (2009). "Characterization of the CO2 fluid adsorption in coal as a function of pressure using neutron scattering techniques (SANS and USANS)." International Journal of Coal Geology **77**(1-2): 69-79.

Melnichenko, Yuri B (2016). Small-Angle Scattering from Confined and Interfacial Fluids Applications to Energy Storage and Environmental Science, Springer.

Melnichenko, Yuri B, Lilin He, Richard Sakurovs, Arkady L Kholodenko, Tomasz Blach, Maria Mastalerz, Andrzej P Radliński, Gang Cheng and David FR Mildner (2012). "Accessibility of pores in coal to methane and carbon dioxide." Fuel **91**(1): 200-208.

Pomme, Stefaan, R Fitzgerald and J Keightley (2015). "Uncertainty of nuclear counting." Metrologia **52**(3): S3.

Radlinski, Andrzej P (2006). "Small-angle neutron scattering and the microstructure of rocks." Reviews in Mineralogy and Geochemistry **63**(1): 363-397.

Radlinski, Andrzej P, Tomasz Blach, Phung Vu, Yeping Ji, Liliana de Campo, Elliot P Gilbert, Klaus Regenauer-Lieb and Maria Mastalerz (2021). "Pore accessibility and trapping of methane in Marcellus shale." International Journal of Coal Geology **248**: 103850.

Radliński, AP, CJ Boreham, P Lindner, O Randl, GD Wignall, A Hinde and JM Hope (2000). "Small angle neutron scattering signature of oil generation in artificially and naturally matured hydrocarbon source rocks." Organic Geochemistry **31**(1): 1-14.

Radlinski, AP, CJ Boreham, GD Wignall and J-S Lin (1996). "Microstructural evolution of source rocks during hydrocarbon generation: a small-angle-scattering study." Physical Review B **53**(21): 14152.

Radlinski, AP, Maria Mastalerz, AL Hinde, Martin Hainbuchner, Helmut Rauch, Matthias Baron, JS Lin, L Fan and P Thiyagarajan (2004). "Application of SAXS and SANS in evaluation of porosity, pore size distribution and surface area of coal." International Journal of Coal Geology **59**(3-4): 245-271.

Radliński, AP, EZ Radlińska, M Agamalian, GD Wignall, P Lindner and OG Randl (1999). "Fractal geometry of rocks." Physical Review Letters **82**(15): 3078.

Rehm, Christine, Alain Brûlé, Andreas K Freund and Shane J Kennedy (2013). "Kookaburra: the ultra-small-angle neutron scattering instrument at OPAL." Journal of Applied Crystallography **46**(6): 1699-1704.

Sakurovs, Richard, Lilin He, Yuri B Melnichenko, Andrzej P Radlinski, Tomas Blach, Hartmut Lemmel and David FR Mildner (2012). "Pore size distribution and accessible pore size distribution in bituminous coals." International Journal of Coal Geology **100**: 51-64.

Sander, Regina, Zhejun Pan and Luke D Connell (2017). "Laboratory measurement of low permeability unconventional gas reservoir rocks: A review of experimental methods." Journal of Natural Gas Science and Engineering **37**: 248-279.

Schmidt, PAUL W (1982). "Interpretation of small-angle scattering curves proportional to a negative power of the scattering vector." Journal of Applied Crystallography **15**(5): 567-569.

Schmidt, Paul W, Axel Höhr, Hans-Bernd Neumann, Helmut Kaiser, David Avnir and Jar Shyong Lin (1989). "Small-angle x-ray scattering study of the fractal morphology of porous silicas." The Journal of chemical physics **90**(9): 5016-5023.

Sieminski, Adam (2021). "EIA's Global Energy Outlook." from https://eneken.ieej.or.jp/data/6999.pdf.

Silva, Tânia LS, Sergio Morales-Torres, Sérgio Castro-Silva, José L Figueiredo and Adrián MT Silva (2017). "An overview on exploration and environmental impact of unconventional gas sources and treatment options for produced water." Journal of environmental management **200**: 511-529.

Sokolova, Anna, Andrew E Whitten, Liliana de Campo, Jason Christoforidis, Andrew Eltobaji, John Barnes, Frank Darmann and Andrew Berry (2019). "Performance and characteristics of the BILBY time-of-flight small-angle neutron scattering instrument." Journal of Applied Crystallography **52**(1): 1-12.

Sun, Mengdi, Jianjiang Wen, Zhejun Pan, Bo Liu, Tomasz P Blach, Yeping Ji, Qinhong Hu, Bingsong Yu, Chunming Wu and Yubin Ke (2022). "Pore accessibility by wettable fluids in overmature marine shales of China: Investigations from contrast-matching small-angle neutron scattering (CM-SANS)." International Journal of Coal Geology: 103987.

Sun, Mengdi, Jianjiang Wen, Zhejun Pan, Bo Liu, Tomasz P Blach, Yeping Ji, Qinhong Hu, Bingsong Yu, Chunming Wu and Yubin Ke (2022). "Pore accessibility by wettable fluids in overmature marine shales of China: Investigations from contrast-matching small-angle neutron scattering (CM-SANS)." International Journal of Coal Geology **255**: 103987.

Sun, Mengdi, Bingsong Yu, Qinhong Hu, Song Chen, Wei Xia and Ruochen Ye (2016). "Nanoscale pore characteristics of the Lower Cambrian Niutitang Formation Shale: a case study from Well Yuke# 1 in the Southeast of Chongqing, China." International Journal of Coal Geology **154**: 16-29.

Sun, Mengdi, Bingsong Yu, Qinhong Hu, Rui Yang, Yifan Zhang, Bo Li, Yuri B. Melnichenko and Gang Cheng (2018). "Pore structure characterization of organic-rich Niutitang shale from China: Small angle neutron scattering (SANS) study." International Journal of Coal Geology **186**: 115-125.

Sun, Mengdi, Bingsong Yu, Qinhong Hu, Yifan Zhang, Bo Li, Rui Yang, Yuri B. Melnichenko and Gang Cheng (2017). "Pore characteristics of Longmaxi shale gas reservoir in the Northwest of Guizhou, China: Investigations using small-angle neutron scattering (SANS), helium pycnometry, and gas sorption isotherm." International Journal of Coal Geology **171**: 61-68.

Sun, Mengdi, Linhao Zhang, Qinhong Hu, Zhejun Pan, Bingsong Yu, Liangwei Sun, Liangfei Bai, Haijiao Fu, Yifan Zhang, Cong Zhang and Gang Cheng (2020). "Multiscale connectivity characterization of marine shales in southern China by fluid intrusion, small-angle neutron scattering (SANS), and FIB-SEM." Marine and Petroleum Geology **112**: 104101.

Sun, Mengdi, Jiale Zhao, Zhejun Pan, Qinhong Hu, Bingsong Yu, Yuling Tan, Liangwei Sun, Liangfei Bai, Chunming Wu and Tomasz P Blach (2020). "Pore characterization of shales: A review of small angle scattering technique." Journal of Natural Gas Science and Engineering: 103294.

Sun, Mengdi, Xiang Zhao, Qing Liu, Chima Finnian Ukaomah, Shu Jiang, Qinhong Hu, Qiming Wang, Tomasz P Blach, Bingsong Yu and Gang Cheng (2021). "Investigation of Microwave Irradiation Stimulation to Enhance the Pore Connectivity of Shale." Energy & Fuels **35**(4): 3240-3251.

Wang, Yamin, Abdulmajeed Lafi Z. Almutairi, Pavel Bedrikovetsky, Wendy A. Timms, Karen L. Privat, Saroj K. Bhattacharyya and Furqan Le-Hussain (2022). "In-situ fines migration and grains redistribution induced by mineral reactions – Implications for clogging during water injection in carbonate aquifers." Journal of Hydrology **614**: 128533.

Warpinski, Norman Raymond, Michael J Mayerhofer, Michael C Vincent, Craig L Cipolla and EP Lolon (2009). "Stimulating unconventional reservoirs: maximizing network growth while optimizing fracture conductivity." Journal of Canadian Petroleum Technology **48**(10): 39-51.

Winans, Randall E and P Thiyagarajan (1988). "Characterization of a solvent-swollen coal by small-angle neutron scattering." Energy & Fuels **2**(3): 356-358.

Wong, Po-zen, James Howard and Jar-Shyong Lin (1986). "Surface roughening and the fractal nature of rocks." Physical Review Letters **57**(5): 637.

Wood, Kathleen, Jitendra P Mata, Christopher J Garvey, C-M Wu, William A Hamilton, Peter Abbeywick, Daniel Bartlett, Friedl Bartsch, Peter Baxter and Norman Booth (2018). "QUOKKA, the pinhole small-angle neutron scattering instrument at the OPAL Research Reactor, Australia: design, performance, operation and scientific highlights." Journal of Applied Crystallography **51**(2): 294-314.

Xiong, N, D Mannicke, T Lam and N Hauser (2017). "Gumtree Application for Neutron Scattering. Version 1.13." Zenodo: Geneve, Switzerland.

You, Lijun, Yili Kang, Qiang Chen, Chaohe Fang and Pengfei Yang (2017). "Prospect of shale gas recovery enhancement by oxidation-induced rock burst." Natural Gas Industry B **4**(6): 449-456.

Zhang, Rui, Shimin Liu, Lilin He, Tomasz P Blach and Yi Wang (2020). "Characterizing anisotropic pore structure and its impact on gas storage and transport in coalbed methane and shale gas reservoirs." Energy & Fuels **34**(3): 3161-3172.

Ncnr.nist.gov. 2021. Neutron Activation and Scattering Calculator. [online] Available at: <https://www.ncnr.nist.gov/resources/activation/index.html?cutoff=0> [Accessed 21 August 2022].